Available online at www.sciencedirect.com
ScienceDirect
Ceramics International 35 (2009) 3301–3312
CERAMICS INTERNATIONAL
www.elsevier.com/locate/ceramint

Early stage cavitation erosion within ceramics—An experimental investigation

G. García-Atance Fatjó [a,*], M. Hadfield [a], C. Vieillard [b], J. Sekulic [b]

[a] *Sustainable Design Research Centre, School of Design, Engineering and Computing, Bournemouth University, Poole House, Fern Barrow, Talbot Campus, Poole BH12 5BB, UK*

[b] *SKF Research and Development Company B.V., 3430 DT Nieuwegein, The Netherlands*

Received 30 March 2009; received in revised form 20 April 2009; accepted 23 May 2009
Available online 18 June 2009

Abstract

Six ceramic material types were considered within an experimental investigation to identify the erosion damage mechanisms resulting from cavitation exposure. These materials were a Y-TZP-type zirconia, different commercially available silicon nitrides, a high-purity alumina and a hardened high-nitrogen stainless steel as reference. An ultrasonic transducer was utilised to produce cavitation conditions and the configuration was ''static specimen method'' using a 5-mm diameter probe, 20-kHz and 50-μm amplitude. The exposure times were periods from 15 s to 3 h.

Experimental methods employed to characterise wear mechanisms were light microscopy, scanning light interferometry and scanning electron microscopy.

It was found that the zirconia and silicon nitrides demonstrated evidence of local pseudo-plastic deformation or depression prior to more pronounced erosion damage by fracture. Zirconia showed evidence of delayed surface changes when the sample is at rest stored in air, possibly by spontaneous phase transformation after the completion of the erosion tests. Alumina showed evidence of brittle surface fracture and negligible or no pseudo-plastic deformation. All wear mechanisms are discussed, and the materials are ranked in terms of cavitation resistance performance.

Keywords: C. Plasticity; C. Toughness and Toughening; D. Si_3N_4; D. ZrO_2

1. Introduction

Cavitation erosion behaviour of ceramics has been studied traditionally from the point of view of material loss rate and incubation time [1–3]. Incubation time has been measured as the time when a weight loss of 0.1 mg is detected [1]. This approach is suitable in applications where the form keeping is a critical factor.

There are some applications where ceramics are used in such condition that keeping the roughness is a key factor and where cavitation can be a determining factor to produce erosion. An example of this application is ceramic bearings working in low saturation lubricants. Not too much work has studied the materials' behaviour in the early stages of cavitation erosion in ceramics. Haosheng et al. study the damage on steel surface at the incubation stage of cavitation erosion. They show the mechanisms of plastic deformation crater with brittle fracture due to shear waves. These craters are about three microns depth [4,5].

There have also been studies focussing on the cavitation itself [6]. Moussatov et al. has studied about the cone-like bubble formation that occurs when there is no stationary specimen in front of the probe [7] and ultrasonic cavitation in thin liquid layers [8] that is important in this study due to its relation with the configuration of the test that has been used. Moussatov shows that there is an amplification factor in the cavitation produced in the central point of a cylindrical thin layer by means of an ultrasonic device.

Within this study, comparison of ceramic material and stainless steel cavitation erosion behaviour in early stages has been carried out. The initial plastic deformation due to the shock pressure plays an important role in the mechanism of damage. A ranking system of the materials performance has been created.

* Corresponding author. Tel.: +44 1202 965079; fax: +44 1202 965314.
E-mail address: ggafatjo@bournemouth.ac.uk (G. García-Atance).

0272-8842/$36.00
doi:10.1016/j.ceramint.2009.05.020

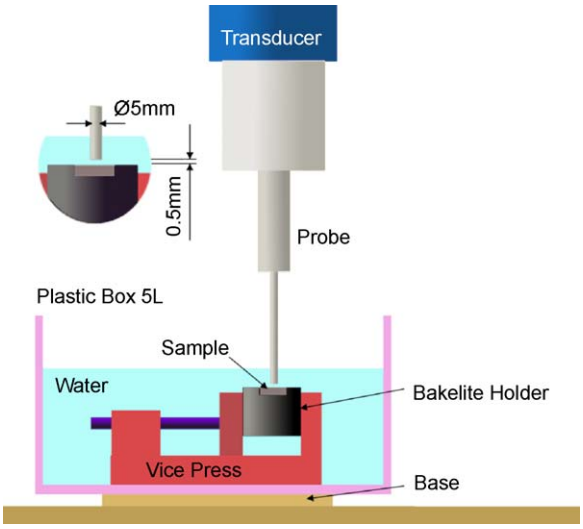

Fig. 1. Test assembly.

2. Testing methodology

The testing methodology is based on the standard ASTM G32-03 [9]. This standard defines the method to test cavitation erosion in brittle materials also referred as "stationary specimen method". The methodology followed in this paper has one difference related to the standard. The standard defines a probe diameter of 15.9 mm, while in these experiments the probe diameter is 5 mm. This configuration with different probe diameters has been studied in [8]. It was reported that there are some diameters that produce magnification of the pressure due to geometrical amplification factors. The geometry chosen in this study does not present this magnification and creates a slow damage rate that is useful to study the mechanism of erosion. Fig. 1 shows the test assembly. The gap between the probe and the sample is 0.5 mm and the specimens are flat. Table 1 shows the roughness of the samples before tests, all the samples have been polished following the same method, with diamond slurry.

An ultrasonic piezoelectric transducer has been used. This transducer oscillates at the frequency of 20 kHz and with amplitude of 8.9 μm, whereas the titanium probe has a natural resonance of 20 kHz and a amplitude gain of 5.6 measured with the optical microscope. The oscillation amplitude of the probe tip is 50 μm. The electric working power of the system was approximately 7 W with this configuration and this gap. The ASTM Standard [9] recommends the values of 20 kHz and 50 μm. The water temperature was the room temperature of 22 °C and the depth of the sample was 10 mm.

Optical microscope micrographs were conducted at various cavitation exposure times from 15 s to 180 min. These micrographs are always taken of the same place in the sample in order to identify the changes of the surface. This place corresponds to the point of the sample below the central point of the probe tip in the assembly. A marked and cut acetate sheet is used to locate the position of the probe on the sample and place it under the microscope. Besides the central point marked on the acetate sheet, several characteristic references on the surfaces of the samples were used to locate the samples in the microscope with more precision. These references were close to the border of the visual image within the ocular lens.

With this process, a record of the surface along the cavitation erosion in early states can be made. Micrographs with polarizing filter are useful to note the small initial damage on the surface, because any small change in the slope of the surface is visible with the filter and because damage and/or plastic deformation will create a slope. Micrographs without polarizing filter are useful to note the cracks and material loss.

A Profiler Interferometer has been used to measure the damage on the surface of the samples. Measurements have been taken at 0 s, 60 min and 120 min. The measurements were made for the sample area corresponding to the centre of the cavitation damage (centre corresponding to the probe). Measurements of the pseudo-plastic deformation pits have been made as well. SEM observation of the damaged surface was carried out after 180 min of cavitation exposure.

A ranking was made for the cavitation erosion resistance of the different materials considering several parameters such as plastic deformation pit volume, surface roughness, number of plastic deformation pits and surface loss.

Wettability or contact angle produced by a drop of water on the polished surface of the samples were checked and did not show noticeable difference. With a hydrophobic surface, the existence of a nuclei on the surface where the cavity starts to grow is more likely, and it can collapse close to the surface [10]. The influence of this factor has been rejected as not important due to the similarity of hydrophobic characteristic of the surfaces.

Table 1
Roughness of samples before tests.

	R_a	rms
Alumina	0.019 μm	0.060 μm
Zirconia	0.003 μm	0.004 μm
Silicon Nitride "A"	0.001 μm	0.002 μm
Silicon Nitride "B"	0.003 μm	0.003 μm
Silicon Nitride "C"	0.001 μm	0.003 μm
Silicon Nitride "D"	0.008 μm	0.010 μm
Stainless Steel	0.001 μm	0.001 μm
Definitions	$R_a = \frac{1}{L}\int_0^L \lvert z(x)\rvert dx$	$\text{rms} = \sqrt{\frac{1}{L}\int_0^L z^2(x)dx}$

3. Analysis of results

3.1. Silicon nitride

Silicon nitride from different manufacturers have been tested, see Table 2. Their manufacturing process has yielded a minimum presence of porosity. Fig. 2 shows the grain size for the various materials. Silicon nitride A shows the finest average grain size. Silicon nitride B and C are similar to each other and slightly coarser than material A. Material D was the coarsest. As shown in Table 2, they show fairly similar hardness and toughness values, when measured with a Vickers hardness method, material D presenting slightly lower hardness and fracture indentation toughness.

Table 2
Silicon nitride material properties. Courtesy of SKF.

	A	B	C	D
Hardness HV10, kg/mm^2	1592	1542	1600	1485
Fracture indentation toughness, MPa $\sqrt{m}$	7.02 ± 0.10	6.9 ± 0.30	7.3 ± 0.20	6.23 ± 0.05
Bending strength, MPa (Weibull modulus)	1174 (16.3)	956 (13.5)	1043 (16.6)	816 (25)

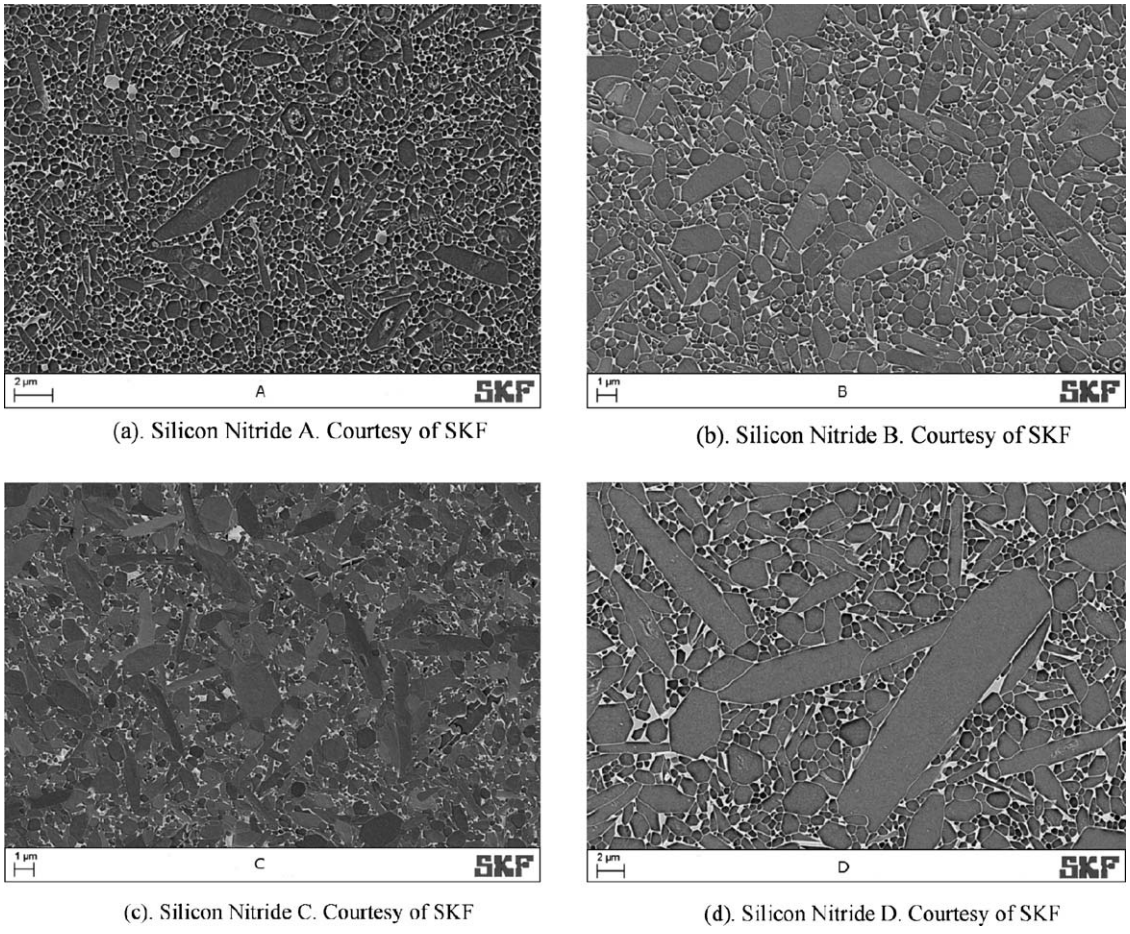

(a). Silicon Nitride A. Courtesy of SKF

(b). Silicon Nitride B. Courtesy of SKF

(c). Silicon Nitride C. Courtesy of SKF

(d). Silicon Nitride D. Courtesy of SKF

Fig. 2. (a) Silicon Nitride A. Courtesy of SKF; (b). Silicon Nitride B. Courtesy of SKF; (c). Silicon Nitride C. Courtesy of SKF; (d). Silicon Nitride D. Courtesy of SKF.

Fig. 3 shows the damage produced in the silicon nitride ''A'' in the first 15 s of cavitation exposure. They consist in few small pits shown by a black arrow. The pits that are not labelled with a small black arrow were present before tests and can be the results of the sample polishing.

Fig. 4 shows the measurement with an interferometer profiler of a plastic deformation pit produced in the first minute. The largest pits can have dimensions of up to 0.05–0.09 μm depth and diameters of 8–12 μm depending on the silicon nitride material and the pit. Typical diameters of the jet stream in a collapsing bubble are about 4 μm for bubbles of 200 μm diameter [4]. This value is consistent with the size of the damage.

Fig. 5 shows three typical pits of the early erosion damage seen with polarizing filter with two magnifications. They are indicated with circles. The contrast produced by the slope of the plastic deformation is very obvious at low magnification with polarizing filter but it is not so evident at high magnification, this is an optical effect. It is possible to observe at high magnification that no material loss, in terms of grain pull-out, break-outs or complete dislodging has occurred yet. These pits could be local shallow surface pseudo-plastic deformation creating a slight surface depression visible under the optical microscope with polarizing filter. These surface local depressions or pseudo-plasticity pits are a result of pseudo-plasticity deformation under the pressure of a large bubble collapsing. Observation at high magnification showed that there could be some microcrack on the surface corresponding to the edges of the depressed region from cavitation compression pressures or from shock waves.

Fig. 6 shows the surface of the silicon nitride ''A'' eroded after 180 min of cavitation erosion as opposed to Fig. 5(b) after 2.5 min. The surface has experienced material loss, with small

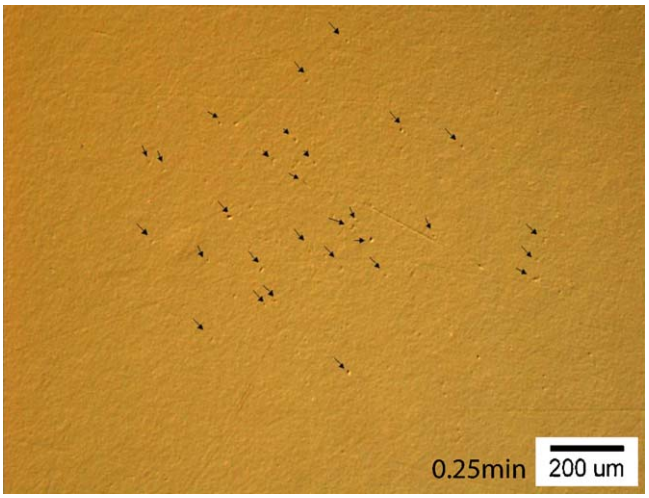

Fig. 3. Pseudo-plastic deformation pits in silicon nitride "A" that have been produced in 15 s of cavitation exposure. Optical microscope.

surface break-outs clustered, where several grains have been pulled out, dislodged from the surface. The rest of the surface shows evidence of smaller isolated grain pull-outs or grain in the process of being dislodged from the surface and possible intergranular cracking.

All surface features have been produced by cavitation, as the original surface was devoid of any of these features. SEM observation of these features was also performed and it is shown in Fig. 7. The damage is mostly intergranular cracking, partial and complete dislodging and pull-outs of single grains or cluster of grains. When damage is initiated, new roughness due to missing surface grain enhances the severity of erosion and further wear around the first damage nuclei.

3.2. Zirconia

The zirconia material was a commercially available Y-TZP material, manufactured by sintering, and hot isostatic pressing providing a fine structure, high density, with a fine distribution of very small alumina based secondary phase and a dual distribution of very fine zirconia grains (submicron or about 1 μm) and few coarser zirconia grains (from 3 to 5 μm diameter), as shown in Fig. 8. Table 3 indicates the measured properties.

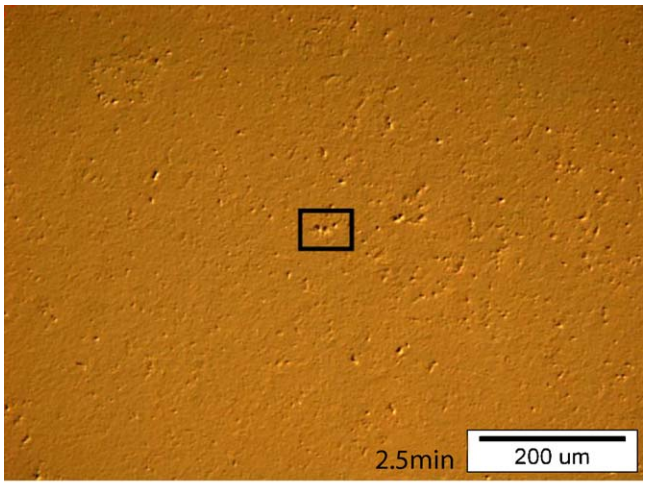

(a). Pseudoplastic deformation pits in silicon nitride "B" that have been produced in 2.5 minutes of cavitation exposure. Optical microscope

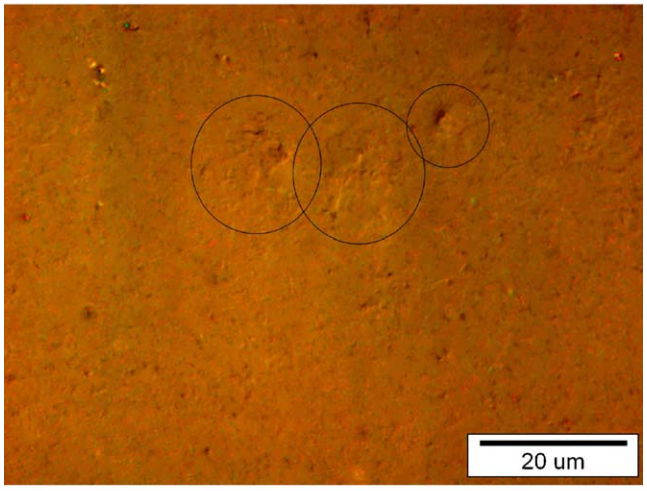

(b). High magnification of the indicated zone of Fig. 5(a). Optical microscope

Fig. 5. (a) Pseudo-plastic deformation pits in silicon nitride "B" that have been produced in 2.5 min of cavitation exposure. Optical microscope; (b). High magnification of the indicated zone of (a). Optical microscope.

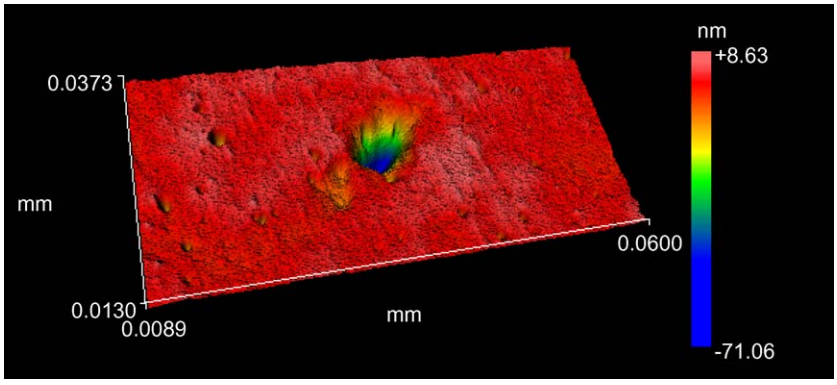

Fig. 4. Pseudo-plastic deformation pit in silicon nitride "A" that has been produced in 1 min of cavitation exposure. Interferometer measurement.

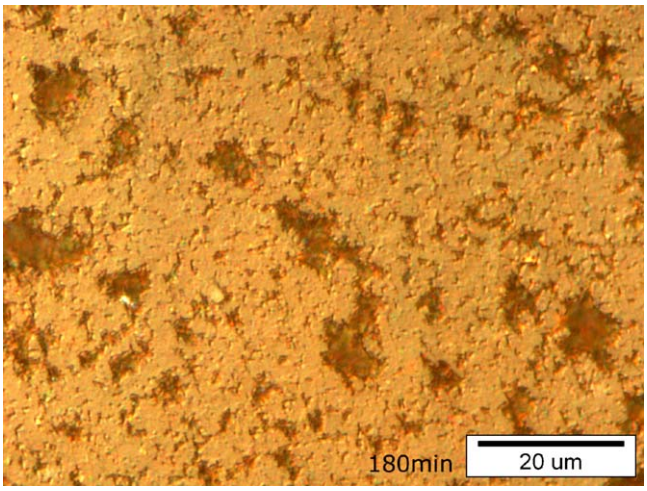

Fig. 6. Surface damage on silicon nitride "A" after 180 min. Optical microscope.

Zirconia presents the best cavitation erosion resistance behaviour among the ceramic materials studied here. Four small pseudo-plasticity pits have been seen in the first 30 s of cavitation erosion test, and this number increased proportionally with the time. These pseudo-plasticity pits are similar to those shown on the surface of silicon nitride but tend to be smaller than those of silicon nitride and their formation is more unlikely than in silicon nitride. The largest pits can have dimensions of up to 0.03–0.05 μm depth and diameters of 3–6 μm. The same impact pressure from a collapsing bubble is more likely to produce a pseudo-plasticity pit in silicon nitride than in zirconia since the pressure threshold to produce the pit is smaller in silicon nitride than in zirconia.

Fig. 9 shows the erosion damage after 180 min of test with visible material loss.

The process of material loss consists of the following: the pressure and the pseudo-plastic deformations create cracks that

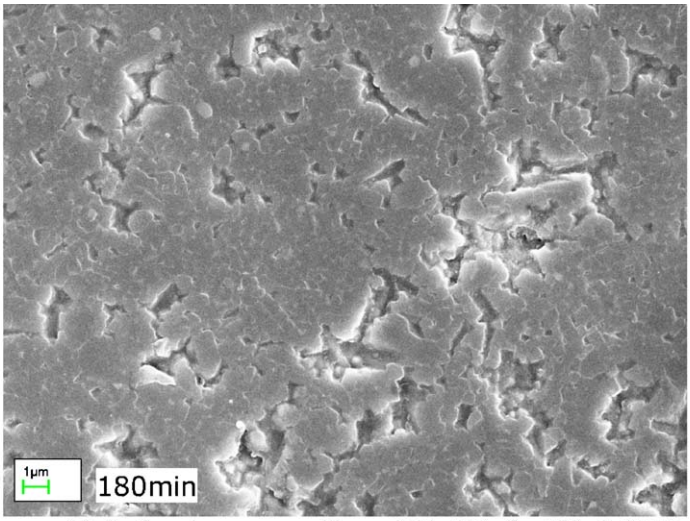

(a). Surface damage on a silicon nitride "A" after 180min.SEM.

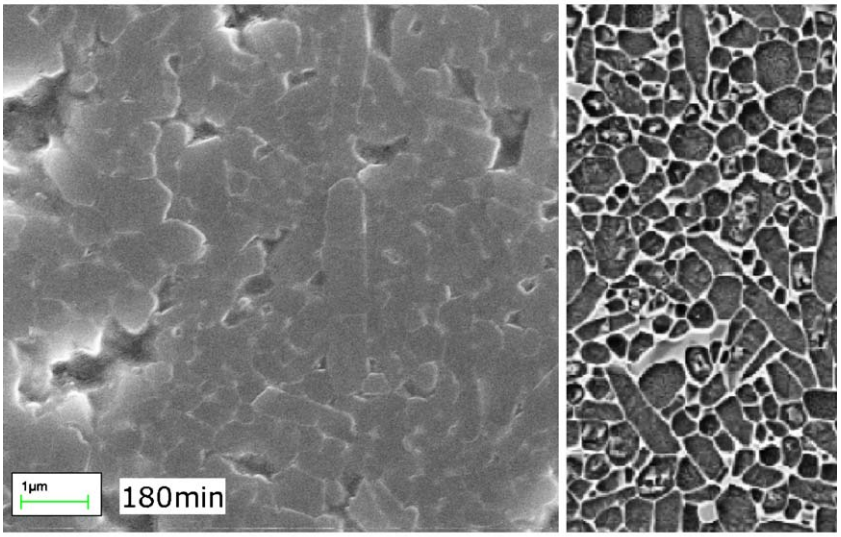

(b). Surface damage on a silicon nitride "A" after 180 min.
Comparison with microstructure Fig 2(a). SEM.

Fig. 7. (a) Surface damage on a silicon nitride "A" after 180 min. SEM. (b) Surface damage on a silicon nitride "A" after 180 min. Comparison with microstructure Fig. 2(a). SEM.

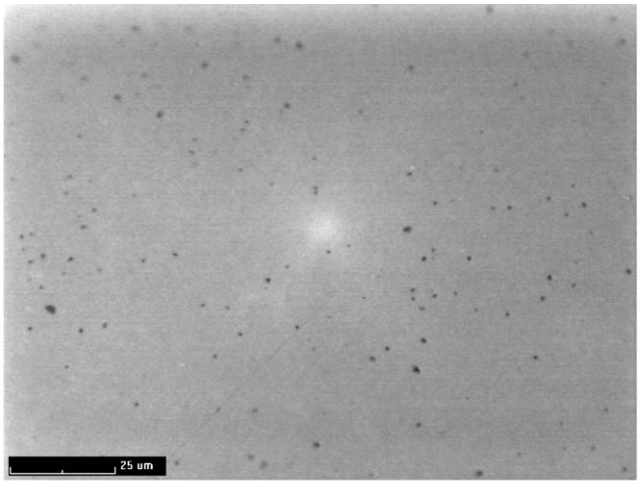

(a). Polished Zirconia Y-TZP. Courtesy of SKF

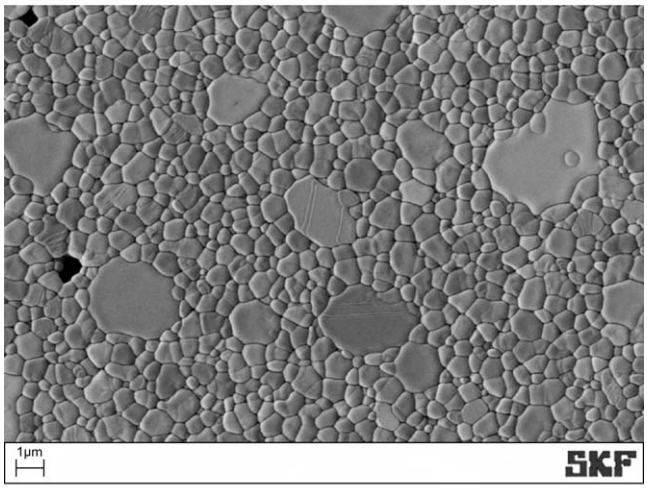

(b). Thermal etched Zirconia Y-TZP. Courtesy of SKF

Fig. 8. (a) Polished Zirconia Y-TZP. Courtesy of SKF; (b) Thermal etched Zirconia Y-TZP. Courtesy of SKF.

Table 3
Zirconia material properties. Courtesy of SKF.

	Hardness HV10, kg/mm^2	Fracture indentation toughness, MPa $\sqrt{m}$	Conventional bending strength, MPa (Weibull Modulus)
Y-TZP Zirconia	1271	10.51	1418 (16.1)

with the time dislodge grains from the surface and can lead to larger local break-outs (Fig. 10).

The zirconia was based on the tetragonal phase, metastable phase, stabilised at room temperature by the yttria dopant. This phase can change and transform back into the stable monoclinic phase at room temperature when subjected to enough pressure and in presence of water [11]. Upon phase transformation, the grain undergoes a small volume increase. The relation of this with the cavitation resistance has been studied in [12]. It was found that in fact there is a change of phase and transformation toughening in zirconia when it is exposed to cavitation.

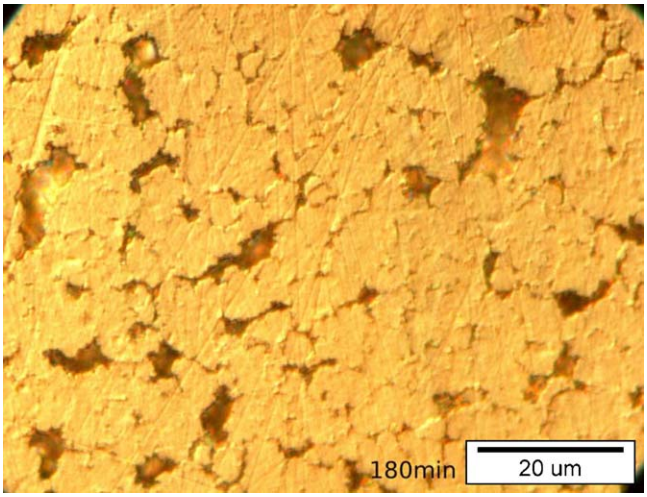

Fig. 9. Zirconia. Surface damage. Optical microscope.

The present study has found out that the surface can change just with the time after the end of the erosion test, when the sample is stored at room temperature in air. Fig. 11(a) shows the surface after 40 min of cavitation exposure. Fig. 11(b) shows exactly the same surface that Fig. 11(a) two months later. The surface has changed. It is possible to look at the same points in both micrographs using the polishing lines as references. The surface develops a topography with small local protruding areas. This suggests that the metastable tetragonal phase can transform spontaneously into the monoclinic in time when stored at rest in air and room temperature after being ''activated'' with cavitation. This transformation occurred at room temperature.

The roughness of the sample has been measured in a region exposed to cavitation for 40 min one day after and eleven days after, and in other region exposed to cavitation for the same time two months ago. These values are shown in Table 4.

In order to check if the transformation creates bulging of the surface due to volume increase and if it does not produce real cracking and grain dislodging several high magnification micrographs of this process have been taken after 40 and 120 min of cavitation exposure. Fig. 12 shows that the principal characteristic of this transformation is bulging of the surface and the existing cracks become more visible than before. In this case, the changes of the surface seems to be smaller than before due to polarizing filter does not show the slopes of the surface in an evident way with high magnification.

3.3. Alumina

The alumina material was a 99.9% purity commercially available pressure-less sintered alumina showing noticeable porosity with a size up to 20 µm, and grain size up to 8 µm as shown in Fig. 13. The polished specimen for the erosion test presented more small break-outs than the genuine material porosity. Table 5 indicated the measured properties.

Alumina cavitation erosion showed a few number of points with change of slope in the first 30 s. This is not clear if it is due to pseudo-plasticity pits or direct brittle fracture dislodging

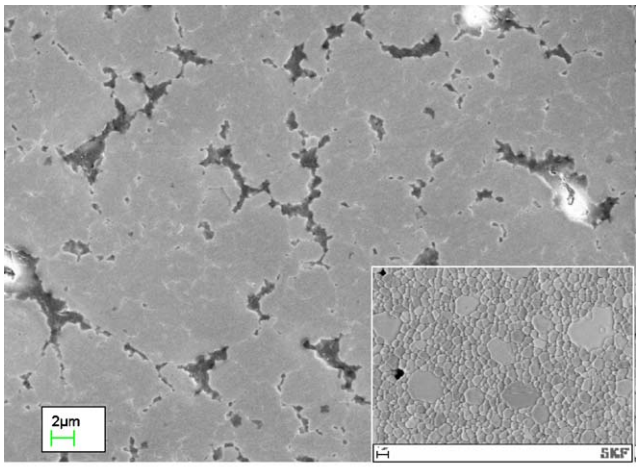

(a). Zirconia. Surface damage after 180 minutes. Comparison with microstructure. SEM.

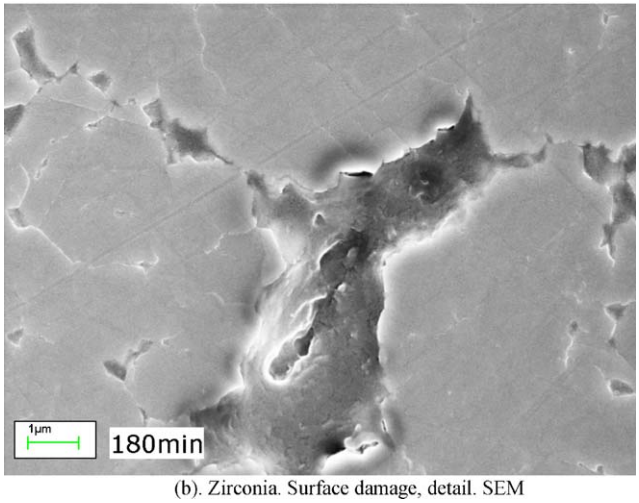

(b). Zirconia. Surface damage, detail. SEM

Fig. 10. (a) Zirconia. Surface damage after 180 min. Comparison with microstructure. SEM. (b). Zirconia. Surface damage, detail. SEM.

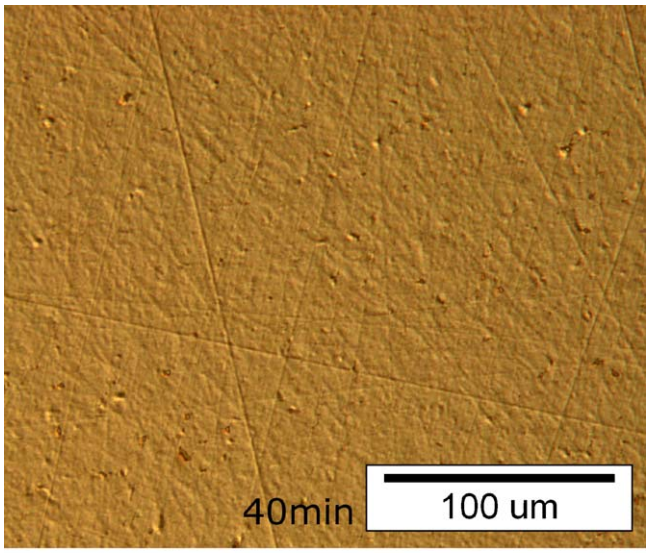

(a). Zirconia. Surface state after the experiment. Optical microscope.

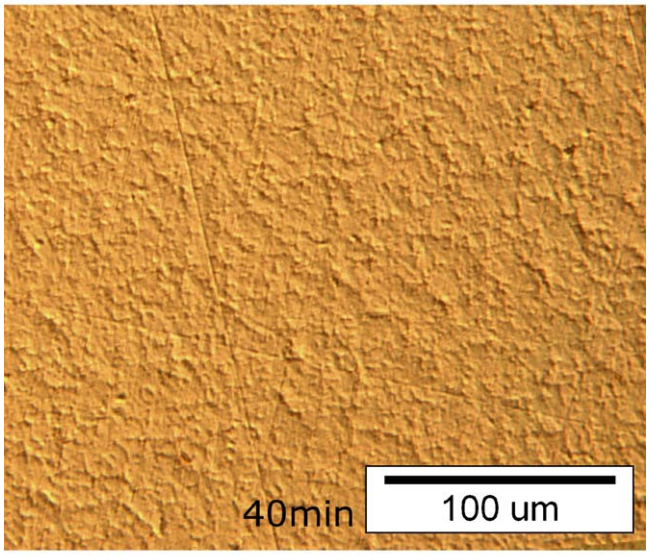

(b). Zirconia. Surface state 2 months after the experiment. Optical microscope.

Fig. 11. (a) Zirconia. Surface state after the experiment. Optical microscope. (b) Zirconia. Surface state two months after the experiment. Optical microscope.

grains at the surface. These features were very small in comparison with the ones visible in other materials. Very quickly with testing time, intergranular micro-cracks appear and grow, especially close to holes from the finishing. These cracks lead to grain pull-outs and larger break-outs in the first minute of tests. Fig. 14(a) and (b) shows the micro-cracks and the grain pull-outs and larger break-outs after 6 and 10 min of tests in the same region. The mechanism of erosion of the alumina is different from the other materials.

3.4. Stainless steel

The stainless steel sample was a nitrogen martensitic stainless steel with a Vickers hardness of HV10 of 734 kg/mm^2.

The stainless steel behaviour under cavitation erosion test is completely different from the ceramic materials due to its capability of plastic deformation and work-hardening. The plastic deformation in its surface is pronounced and accumulated with testing time. It starts in the first few seconds and extends with the time. To see the plastic deformation pits isolated from each other is necessary to stop the transducer in the first seconds. This study has done it after two seconds, in order to measure the volume of the pits with respect to the original surface.

The number of plastic deformation pits over a determined area increased quickly in the first minute. These pits were

Table 4
Zirconia, change of roughness with the time after 40 min of cavitation exposure. The surface has been "activated".

	R_a (µm)	rms (µm)
Region "A" after one day	0.004	0.006
Region "A" after eleven days	0.006	0.010
Region "B" after two months	0.008	0.011

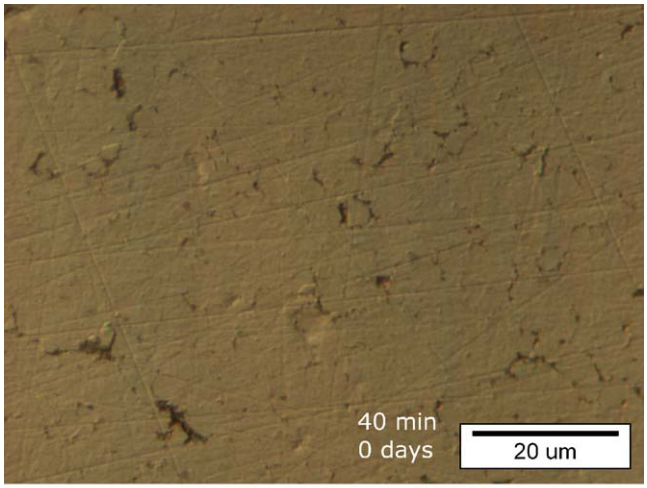

(a). Zirconia. Surface state after the experiment. Optical microscope.

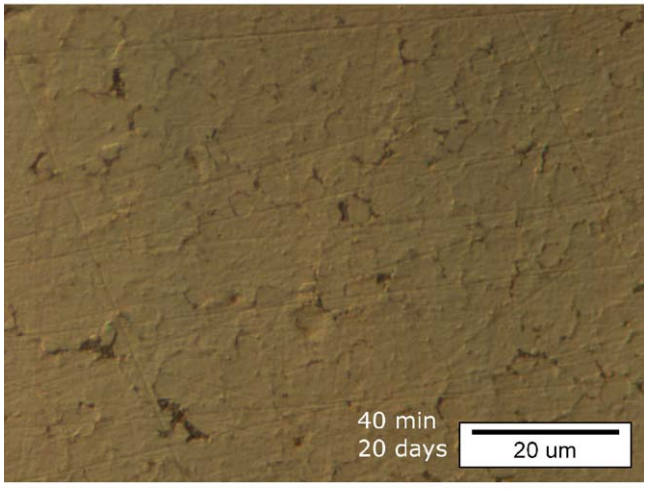

(b). Zirconia. Surface state after the experiment. Optical microscope.

Fig. 12. (a) Zirconia. Surface state after the experiment. Optical microscope. (b) Zirconia. Surface state 20 days after the experiment. Optical microscope.

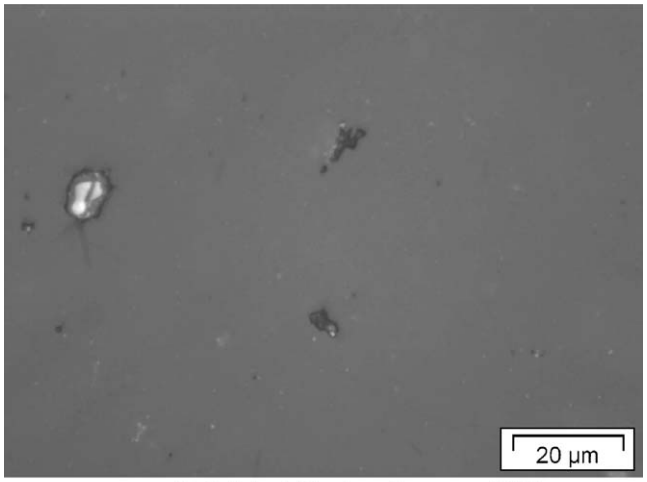

(a). Polished Alumina. Courtesy of SKF

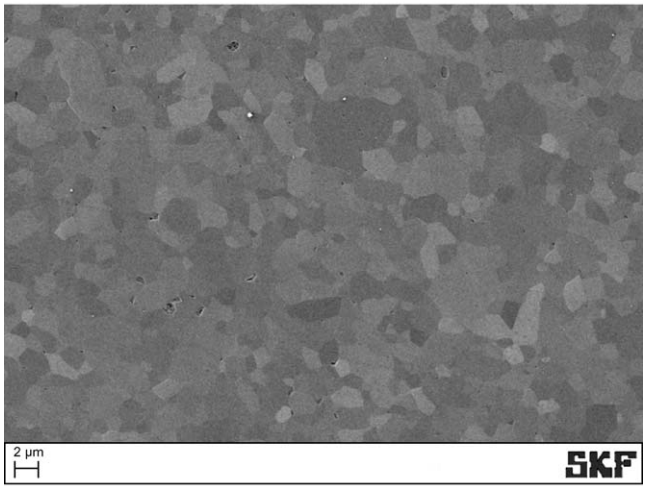

(b). Microstructure of the Alumina. Courtesy of SKF

Fig. 13. (a) Polished Alumina. Courtesy of SKF; (b) Microstructure of the Alumina. Courtesy of SKF.

clearly larger than those from other materials. The largest pits can have dimensions of up to 0.08–0.15 μm depth and diameters of 11–15 μm. After the first minute the number of pits increased but these pits were smaller with the time. Fig. 15 shows the damage progress. This effect is produced because of the work-hardened of the surface produced by accumulated plastic deformation.

The typical form of the plastic deformation pit is shown in Fig. 16. This shows that there is no accumulation of material on the sides of the pit, thus, the pit is so shallow that the material, probably, has been just compressed towards inside of the surface, orthogonal to this without creating apparently raised edges from elastic relaxation, but this could be hidden because of the different magnification scale of the image in vertical and horizontal axis, because of the very small depth of the pit, 88 nm and because of the elastic properties of the material surrounding that can absorb the small deformation.

A different colour has appeared in the region of more severe cavitation erosion during the second hour of cavitation exposure in the micrographs. Although it may be possible to think that this colour is due to oxidation because of the high temperatures that cavitation can achieve, the analysis of elements in the scanning electron microscope has not shown evidence of oxygen in the region. Fig. 17 shows this coloured effect. On the other hand, identification of material loss was not possible by using microscopy due to the high undulation of the surface because of deformation.

Table 5
Alumina material properties. Courtesy of SKF.

	Hardness HV10, kg/mm^2	Fracture indentation toughness, MPa $\sqrt{m}$	Conventional bending strength, MPa (Weibull Modulus)
Alumina	1828	3.77	~300 (8.1)

3.5. Rankings

In order to create a ranking of the materials and to obtain a better understanding of the mechanisms of cavitation erosion of these materials, several criterions have been followed. Table 6 shows the volume and the depth of a typical pseudo-plastic

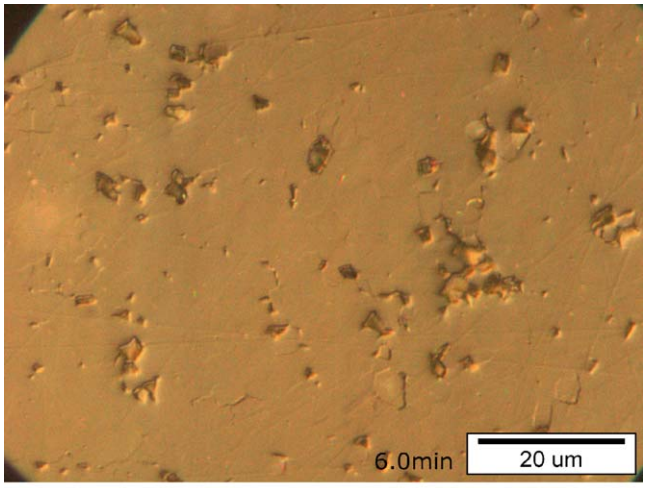

(a). Alumina. Cracks and grain pull-outs (6 minutes). Optical microscope.

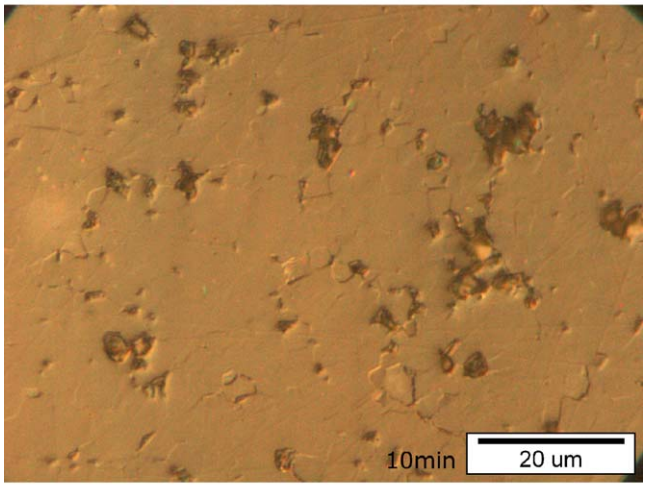

(b). Alumina. Cracks and grain pull-outs (10 minutes). Optical microscope.

Fig. 14. (a) Alumina. Cracks and grain pull-outs (6 min). Optical microscope. (b) Alumina. Cracks and grain pull-outs (10 min). Optical microscope.

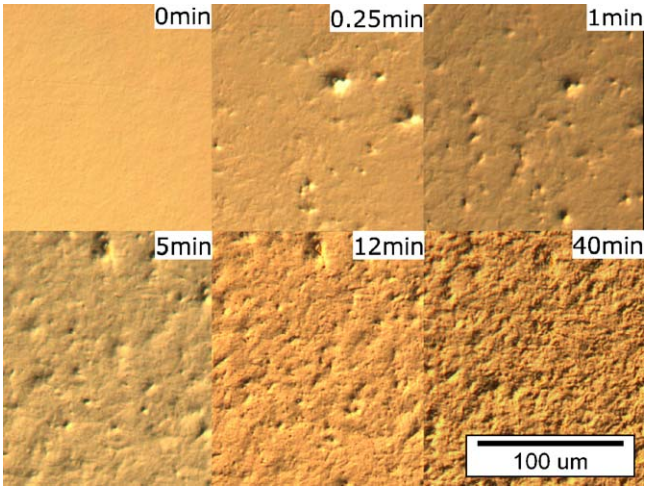

Fig. 15. Stainless steel. Plastic deformation. Optical microscope.

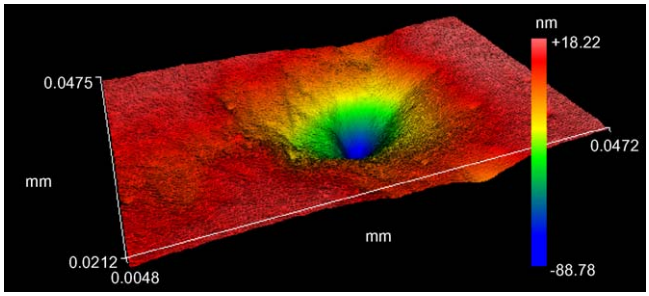

Fig. 16. Plastic deformation pit in Stainless Steel that has been produced in two seconds of cavitation exposure. Interferometer measurement.

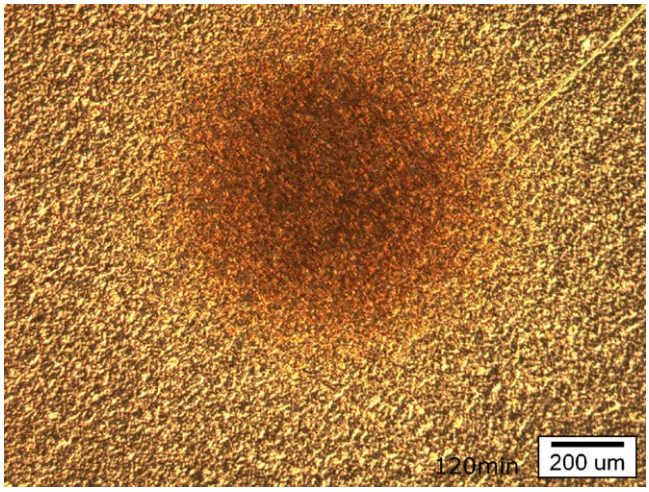

Fig. 17. Cavitation erosion region after 120 min of cavitation exposure. Optical microscope.

Table 6
Measurement averages of pseudo-plastic deformation pits with profiler interferometer.

	Time of measurement	Typical volume (μm^3)	Typical depth (μm)
Alumina	–	Not measurable	Not measurable
Zirconia	4 min	0.6	0.03
Silicon Nitride, "A"	1 min	1.7	0.05
Silicon Nitride, "C"	0.5 min	2.0	0.06
Silicon Nitride, "D"	1 min	2.2	0.08
Silicon Nitride, "B"	2 min	3.3	0.09
Stainless Steel	2 s	10.0	0.13

deformation pit visible with polarizing filter and low magnification in optical microscope. It has been measured with interferometer profiler at maximum magnification and the result shown is an average of at least three different pits for each material. Some examples of these pits are in Figs. 4 and 16.

Table 7 shows the surface roughness after 120 min of cavitation exposure. The table has been ordered from smaller to greater roughness.

Table 8 shows the number of plastic deformation pits that have been possible to count using optical microscope after 30 s of cavitation exposure. In case of alumina it is not clear if this is pseudo-plasticity pits or slope change due to immediate

Table 7
Surface roughness after 120 min to cavitation exposure.

	R_a (μm)	rms (μm)
Silicon Nitride "A"	0.007	0.020
Zirconia (after eleven days)	0.014	0.048
Zirconia (after three months)	0.019	0.065
Zirconia (after one day)	0.032	0.158
Stainless Steel	0.153	0.206
Silicon Nitride "C"	0.527	0.670
Silicon Nitride "B"	0.654	0.913
Silicon Nitride "D"	1.083	1.324
Alumina	1.138	1.437

Table 8
Number of plastic deformation pits produced in the surface after 30 s of cavitation exposure.

Material	Pits (number)
Zirconia	4
Alumina	7
Silicon Nitride "A"	62
Silicon Nitride "B"	62
Silicon Nitride "D"	77
Silicon Nitride "C"	89
Stainless Steel	Massive

Table 9
Surface loss after 120 min to cavitation exposure.

Material	Surface loss (area), mm^2
Silicon Nitride "A"	0.006
Zirconia	0.015
Silicon Nitride "B"	0.308
Silicon Nitride "D"	0.450
Silicon Nitride "C"	0.548
Alumina	>1.067

fracture/partial grain dislodging. This measurement has been made summing the pits produced in the first 15 s plus the pits produced from 15 to 30 s. The number of pits was similar in both times.

Table 10
Surface loss after 180 min to cavitation exposure.

Material	Surface loss (area), mm^2
Zirconia	0.091
Silicon Nitride "A"	0.144

Table 9 shows the surface that has been removed due to cavitation erosion after 120 min of exposure. To calculate this, the micrographs have been processed with image software. The micrographs that have been taken without polarizing filter have been transformed in images of two colours, black and white, changing the brightness and the contrast, and the number of black pixels has been counted with the software. As the size of the pixel is known, the area of surface loss has been calculated. The processed micrographs are shown in Fig. 18. Table 10 shows the comparison of silicon nitride "A" and Zirconia in a later state, after 180 min of exposure. In this stage Zirconia has a better result.

4. Discussion

The initial surface roughness of the sample depends on the mechanical properties of the surface and its characteristics since all the samples have been polished in the same way. The alumina sample had an initial rougher surface due to the larger and higher porosity presence as well as some break-outs at pores during polishing.

When ceramics materials are exposed to cavitation, pseudo-plastic deformation pits are created on the surface. In the case of alumina, that is more brittle than the others, intergranular fracture occurs and material loss is produced quickly, Fig. 14. Although some small changes of slope have been seen in alumina, this is not clear if they are produced by pseudo-plastic deformation, by fracture or by both. Silicon nitride and zirconia stand some initial pseudo-plastic deformation but it is accompanied by limited cracking in the vicinity of the depressed area Fig. 5(b). Upon further cavitation, these cracks

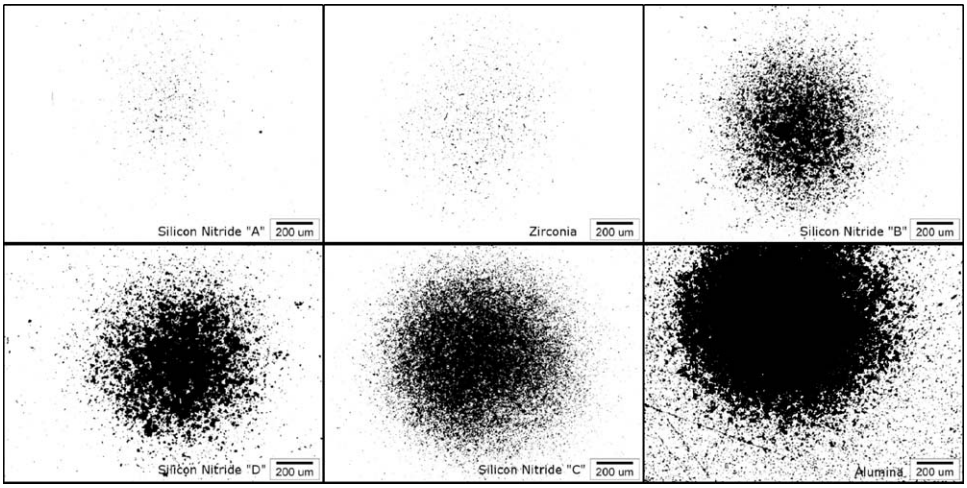

Fig. 18. Surface loss after 120 min to cavitation exposure. Processed micrographs.

may grow or due to the roughness increase, more severe cracking occurs leading the first grain dislodging and pull-outs. With further cavitation time the small pits of missing grains extend by eroding edge grains, forming larger break-outs (Figs. 6, 7, 9 and 10).

It is considered that tetragonal to monoclinic phase transformation occurred after the cavitation erosion test once the sample is at rest in ambient air at room temperature. During cavitation, pseudo-plastic deformation occurs; higher compressive residual stress may be produced at the surface and this leads to some spontaneous phase transformation at the surface of the sample in a natural humid air and with time. This process takes several weeks. This mechanism produced confusion in the results related with zirconia because two different effects play an important role: the cavitation erosion itself with resulting damage just after the test and longer time surface change even if erosion is not acting any more. It has been observed that the phase transformation produces a change in the surface characteristics with time, without more cavitation exposure. This effect has increased the roughness measured with interferometry at 40 min of cavitation exposure but it has decreased the roughness at 120 min of cavitation exposure (Tables 4 and 7).

In the case of stainless steel, larger bubbles collapsing close to the surface created the larger pits at the beginning, when the surface was not work-hardened. While this happens, other smaller bubbles collapsed as well and produced plastic deformation on the surface. The result was a work-hardening of the surface with pits whose size depends on the flux of energy of the collapsing bubble and the local state of the surface (Fig. 15). The important contribution of this part to the understanding of the behaviour of the other materials is that there is a large range of severity in the energy flux of the bubbles collapsing close to the surface. In Table 6 the volume that is measured is the volume of the typical large pits observed with an optical microscope and interferometer profiler. Table 7 shows that the number of damage produced by cavitation is much smaller in zirconia and alumina over the first 30 s. This means that only the collapsing of bubbles that hit with an amount of energy above a threshold creates a permanent effect on the surface. This threshold is higher for zirconia and alumina than for silicon nitride.

Although alumina has less number of pits or damages than the other materials in the first 30 s, it is the material with the poorest cavitation resistance. Silicon nitride "A" has a large number of pits in the first 30 s, similar to the other silicon nitrides, but it has much better cavitation resistance in terms of low damage proliferation rate (Table 9). These facts demonstrate that cavitation resistance is related with: (a) how the materials stand the flux of energy of the collapsing bubble and (b) how the materials avoid the propagation of the cracks and the spread of material loss in the border of the cracks. Macroscopic mechanical characteristics of the material may play a secondary role in comparison with microscopic mechanical characteristics of grains and intergranular phase.

Zirconia has demonstrated the best cavitation resistance, followed by one of the commercial silicon nitrides; alumina has the poorest cavitation resistance.

5. Conclusions

Although it is widely believed that the cavitation exposure of ceramics cannot produce plastic deformation or this is negligible, pseudo-plastic deformation pits have been detected with polarizing filter with optical microscope and have been measured with interferometer profiler in silicon nitride and in zirconia.

Pseudo-plastic deformation pits play a key role in the way of the material to resist cavitation erosion. Alumina, that cannot absorb energy through plastic deformation, suffers fracture from initial exposure and leads quickly to small surface break-outs or grain pull-out. Conversely the absorption of energy by means of plastic deformation in silicon nitride and zirconia allows delaying the creation of big fractures and cracks that cause the material loss.

The change of phase in zirconia from metastable tetragonal to monoclinic with the corresponding volume increase is not an instantaneous effect, but this effect takes several weeks to happen after the surface being exposed to cavitation at room temperature. In the zirconia studied, changes have been seen after two months. This effect, used for transformation toughening in these materials, is caused by the pressure. When the surface is exposed to cavitation, pseudo-plastic deformation is produced on the surface, this induces residual stress. This residual stress "activates" the surface, which leads to the change of phase in the future.

Plastic deformation pit size in stainless steel depends on the local state of the surface due to the work-hardening produced by plastic deformation caused by bubbles that have collapsed previously.

Intergranular material and the way that it can accommodate plastic deformation in the surroundings and in itself have a fundamental role in the cavitation erosion resistance performance.

References

[1] W.J. Tomlinson, S.J. Matthews, Cavitation erosion of structural ceramics, Ceramics International 20 (1994) 201–209.
[2] W.J. Tomlinson, N. Kalitsounakis, G. Vekinis, Cavitation erosion of aluminas, Ceramics International 25 (1999) 331–338.
[3] D. Niebuhr, Cavitation erosion behavior of ceramics in aqueous solutions, Wear 263 (2007) 295–300.
[4] C. Haosheng, L. Jiang, C. Darong, W. Jiadao, Damages on steel surface at the incubation stage of the vibration cavitation erosion in water, Wear 265 (2008) 692–698.
[5] C. Haosheng, L. Shihan, Inelastic damages by stress wave on steel surface at the incubation stage of vibration cavitation erosion, Wear (2008), doi:10.1016/j.wear.2008.05.011.
[6] F. RonaldYoung, Cavitation, Imperial College Press, 1999ISBN 1-86094-198-2.
[7] A. Moussatov, C. Granger, B. Dubus, Cone-like bubble formation in ultrasonic cavitation field, Ultrasonics Sonochemistry 10 (2003) 191–195.
[8] A. Moussatov, C. Granger, B. Dubus, Ultrasonic cavitation in thin liquid layers, Ultrasonics Sonochemistry 12 (2005) 415–422.

[9] ASTM G32-03, Standard Test Method for Cavitation Erosion Using Vibratory Apparatus, ASTM, 2003.
[10] C. Haosheng, L. Jiang, L. Fengbin, C. Darong, W. Jiadao, Experimental study of cavitation damage on hydrogen-terminated and oxygen-terminated diamond film surfaces, Wear 264 (2008) 146–151.
[11] Masahiro Yoshimura, Tatsuo Noma, Katsuichi Kawabata, Shigeyuki Somiya, Role of H_2O on the degradation process of Y-TZP, Journal of Materials Science Letters 6 (1987) 465–467.
[12] J. Lu, et al., Microstructural effects on the resistance to cavitation erosion of ZrO_2 ceramics in water, Wear (2008), doi:10.1016/j.wear.2008.04.028.